INTERNATIONAL JOURNAL OF
NUMERICAL ANALYSIS AND MODELING
Volume 17, Number 3, Pages 350–367

EFFICIENT GALERKIN-MIXED FEMS FOR INCOMPRESSIBLE MISCIBLE FLOW IN POROUS MEDIA

WEIWEI SUN AND CHENGDA WU

Abstract. The paper focuses on numerical study of the incompressible miscible flow in porous media. The proposed algorithm is based on a fully decoupled and linearized scheme in the temporal direction, classical Galerkin-mixed approximations in the FE space $(V_h^r, S_h^{r-1} \times \mathbf{H}_h^{r-1})$ $(r \geq 1)$ in the spatial direction and a post-processing technique for the velocity/pressure, where V_h^r and $S_h^{r-1} \times \mathbf{H}_h^{r-1}$ denotes the standard C^0 Lagrange FE and the Raviart-Thomas FE spaces, respectively. The decoupled and linearized Galerkin-mixed FEM enjoys many advantages over existing methods. At each time step, the method only requires solving two linear systems for the concentration and velocity/pressure. Analysis in our recent work [37] shows that the classical Galerkin-mixed method provides the optimal accuracy $O(h^{r+1})$ for the numerical concentration in L^2-norm, instead of $O(h^r)$ as shown in previous analysis. A new numerical velocity/pressure of the same order accuracy as the concentration can be obtained by the post-processing in the proposed algorithm. Extensive numerical experiments in both two- and three-dimensional spaces, including smooth and non-smooth problems, are presented to illustrate the accuracy and stability of the algorithm. Our numerical results show that the one-order lower approximation to the velocity/pressure does not influence the accuracy of the numerical concentration, which is more important in applications.

Key words. Galerkin-mixed FEM, incompressible miscible flow in porous media, fully linearized scheme.

1. Introduction

Numerical study for incompressible miscible flow in porous media plays an important role in many applications, such as reservoir simulations and surface contaminant transport and remediation. In these areas, the incompressible flow is described by the following miscible displacement system

$$\Phi \frac{\partial c}{\partial t} - \nabla \cdot (D(\mathbf{u}) \nabla c) + \mathbf{u} \cdot \nabla c = \hat{c} q^I - c q^P, \tag{1}$$

$$-\nabla \cdot \frac{\mathbf{K}(x)}{\mu(c)} \nabla p = q^I - q^P, \tag{2}$$

with the initial and boundary conditions:

$$\begin{aligned} &\mathbf{u} \cdot \mathbf{n} = 0,\ D(\mathbf{u}) \nabla c \cdot \mathbf{n} = 0 \quad \text{for } x \in \partial\Omega,\ t \in [0, T], \\ &c(x, 0) = c_0(x) \qquad\qquad\qquad\ \text{for } x \in \Omega, \end{aligned} \tag{3}$$

where $\mathbf{u}$ denotes the Darcy velocity of the fluid mixture defined by

$$\mathbf{u} = -\frac{\mathbf{K}(x)}{\mu(c)} \nabla p, \tag{4}$$

p is the pressure of the fluid mixture and c is the concentration. Moreover, here $\mathbf{K}(x)$ is the permeability tensor of the medium, $\mu(c)$ is the concentration-dependent viscosity, Φ is the porosity of the medium, q^I and q^P are the given injection and production sources, $\hat{c}$ is the concentration in the injection source, and $D(\mathbf{u}) =$

Received by the editors December 5, 2019 and, in revised form, April 14, 2020.
2000 *Mathematics Subject Classification.* 35R35, 49J40, 60G40.

$[D_{ij}(\mathbf{u})]_{d\times d}$ is the velocity-dependent diffusion-dispersion tensor, which may be given in different forms (see [4, 34] for details). We assume that the system is defined in a bounded domain Ω in $\mathbb{R}^d$ $(d = 2, 3)$ and $t \in [0, T]$.

In the last several decades, numerous effort has been devoted to the development of numerical methods for the system (1)-(4), *e.g.* see [18, 26, 28, 25] for Galerkin FEMs, [7, 9, 10, 13, 30] for Galerkin-mixed methods, [11, 15, 19, 20, 41] for characteristics type methods, [38, 39] for ELLAM and [1, 23, 36] for others. Numerical simulations have been made extensively in various engineering areas [10, 14, 17]. Two review articles for numerical methods in these areas were presented by Ewing and Wang [21] and Scovazzi et al.[35], respectively. Theoretical analysis for the existence of weak solutions of the system was studied by Feng [22], while the existence of classical solutions is unknown so far.

As the system consists of a parabolic concentration equation and an elliptic pressure equation, one should choose a proper approximation to each of these computational components, more precisely the degree of piecewise polynomial used for each component. Since the concentration is the most important physical component, the accuracy of numerical concentration is a major concern in applications. Existing algorithms are mainly based on previous error estimates which however may not be optimal in some sense. Therefore, these algorithms often requires a high computational cost and complicated implementation. Numerical analysis for the system (1)-(4) in two-dimensional space was first presented by Ewing and Wheeler [18] for a standard Galerkin-Galerkin approximation $(c_h, p_h) \in (V_h^r, \widehat{V}_h^k)$ where V_h^r denotes C^0 Lagrange finite element space of piecewise polynomials of degree r and $\widehat{V}_h^k := V_h^k/\{constant\}$. Further analysis for Galerkin-Galerkin FEMs can be found in literature [25, 32, 43]. Due to the nature of discontinuity of the gradient of the pressure and continuity of the Darcy velocity in applications, the Galerkin-mixed method is more popular in many areas. In this method, a standard C^0 Lagrange type approximation $c_h \in V_h^r$ is applied for the concentration equation and a mixed approximation in the Raviart–Thomas finite element space (or other mixed FE space) $(p_h, \mathbf{u}_h) \in S_h^k \times \mathbf{H}_h^k$ is used for the pressure equation. The error estimate was first presented in [12] for a semi-discrete Galerkin-mixed method and later, in [13] for a fully discrete semi-implicit Euler scheme. In [13], the error estimate

$$\|c^n - c_h^n\|_{L^2} + \|p^n - p_h^n\|_{L^2} + \|\mathbf{u}^n - \mathbf{u}_h^n\|_{L^2} \le C(\tau + h_c^{r+1} + h_p^{k+1}) \tag{5}$$

was established for $d = 2$ under the time step restriction $\tau = o(h)$ and an extra spatial mesh condition

$$h_c^{-1} h_p^{k+1} = o(1) \tag{6}$$

where h_c and h_p denote the mesh sizes of FE discretization for the concentration and pressure equations, respectively. Further studies on time step restriction and spatial mesh condition were presented in [7, 10, 26, 28, 32]. Analysis for many other methods can be found in literature [1, 6, 15, 38, 41]. Based on the error estimate (5), it was suggested in [13] to use the finite element space $V_h^r \times S_h^r \times \mathbf{H}^r$ $(k = r > 0)$ and later, such a combination of finite element spaces was used widely in computations. On the other hand, due to the discontinuity of physical parameters in applications, the most popular Galerkin-mixed method is the lowest order one $(r = 1, k = 0)$ [7, 9, 13, 15, 21, 35], *i.e.*, a linear approximation to the concentration and the zero-order Raviart–Thomas approximation to the pressure and velocity. The lowest order Galerkin-mixed method has been widely used in a variety of numerical simulations, *e.g.*, see [13, 17, 19, 35]. In this case, the error estimate (5)

reduces to

$$\|c^n - c_h^n\|_{L^2} + \|p^n - p_h^n\|_{L^2} + \|\mathbf{u}^n - \mathbf{u}_h^n\|_{L^2} \le C(\tau + h_p + h_c^2) \tag{7}$$

and the spatial mesh condition (6) becomes

$$h_c^{-1} h_p = o(1) \tag{8}$$

where the commonly-used mesh $h_p = h_c$ is excluded. The low convergence rate of the method is often a major concern in both analysis and computation. Clearly, the error estimate (7) is not optimal for the concentration in general, while the concentration is a more important physical component in practice. Due to the strong coupling of the system, it was assumed that the one-order lower accuracy of the numerical pressure/velocity may pollute the numerical concentration through the diffusion-dispersion tensor $D(\mathbf{u})$ and the viscosity $\mu = \mu(c)$. The non-optimality of the error estimate (7) had not been addressed until our recent work in [37] where a new and optimal error estimate

$$\|c^n - c_h^n\|_{L^2} \le C(\tau + h^2) \tag{9}$$

$$\|p^n - p_h^n\|_{L^2} + \|\mathbf{u}^n - \mathbf{u}_h^n\|_{L^2} \le C(\tau + h) \tag{10}$$

for $h = h_p = h_c$ was presented for the lowest-order Galerkin-mixed method unconditionally.

This paper focuses on numerical study of Galerkin-mixed FEMs with $k = r - 1$ for solving the system (1)-(4). We make a systematic numerical simulation on incompressible miscible flow in a general case, including the problem in both two- and three-dimensional porous media with smooth and non-smooth solutions and physical parameters. Our numerical results show that such Galerkin-mixed FEMs ($k = r - 1$) give numerical solutions of optimal convergence rates for all three physical components. The methods are more efficient in computation and implementation since a lower order approximation is used in these mixed methods. Moreover, we propose a post-processing technique, with which one can obtain the numerical velocity/pressure of the same order of convergence rate as the numerical concentration at certain time level by resolving the elliptic pressure equation with a high-order mixed method.

The rest of the paper is organized as follows. In Section 2, we introduce fully decoupled and linearized Euler and Crank-Nicolson schemes with Galerkin-mixed approximations in the spatial direction for the system (1)-(4) and a post-processing technique for the velocity/pressure. In Section 3, we study the problems with smooth solutions in both two- and three-dimensional space to confirm theoretical analysis presented in [37] in a more general case and to show the high-order accuracy of numerical pressure/velocity in our algorithm. In Section 4, we present two examples. The first one is defined on a L-shape domain with non-smooth solution due to the singularity around the reentrant corner. Our numerical results on uniform meshes show the optimal convergence rates of the algorithm for all three components based on the regularity of the solution and classical interpolation approximation. With an adaptive local refinement of mesh, the convergence rate of the numerical concentration by the lowest-order Galerkin-mixed method increases from $O(h^{3/2-\epsilon})$ to $O(h^2)$. In all these cases, the one-order lower approximation to the velocity/pressure does not influence the accuracy of the concentration. Moreover, in terms of the proposed post-processing, the algorithm based on the lowest-order Galerkin-mixed method provides the second-order accuracy for all three physical

components. In the second example, a practical model with discontinuous permeability coefficient, large mobility ratios and a point source and sink is simulated in comparison with numerical results obtained by other methods.

2. Galerkin-mixed FEMs

Here we present the commonly-used Galerkin-mixed methods and our algorithms. For simplicity, we introduce some notations below. Let $L^2(\Omega)$ be the standard function space of all the square integrable functions in Ω. We denote the Sobolev spaces by

$$\begin{aligned}
&H^1(\Omega) := \{\, v \in L^2(\Omega) \big|\, \nabla v \in [L^2(\Omega)]^d\} \\
&\widehat{H}^1(\Omega) := H^1(\Omega)/\{constants\} \\
&\mathbf{H}^1(\mathrm{d}iv) := \{\mathbf{v} \in [L^2(\Omega)]^d \,\big|\mathrm{d}iv\mathbf{v} \in L^2(\Omega)\,\} \\
&\mathbf{H}_0^1(\mathrm{d}iv) := \{\mathbf{v} \in \mathbf{H}^1(\mathrm{d}iv)\,|\mathbf{v}\cdot\mathbf{n} = 0 \text{ on } \partial\Omega\,\}\,.
\end{aligned}$$

Let $\mathcal{T}_h$ be a regular triangular partition of Ω with $\Omega = \cup_K \Omega_K$ and the mesh size $h = \max_{\Omega_K\in\mathcal{T}_h}\{\mathrm{diam}\,\Omega_K\}$. Let $\{t_n\}_{n=0}^N$ be a uniform partition in the time direction with the step size $\tau = T/N$ and we denote

$$p^n = p(x,t_n), \quad \mathbf{u}^n = \mathbf{u}(x,t_n), \quad c^n = c(x,t_n)\,.$$

For any sequence of functions $\{f^n\}_{n=0}^N$, we define

$$D_t f^{n+1} = \frac{f^{n+1}-f^n}{\tau}\,.$$

The weak formulation of the system (1)-(4) is to seek the solution $(c,p,\mathbf{u}) \in (H^1, \widehat{H}^1, \mathbf{H}_0^1(\mathrm{d}iv))$ such that

$$\Big(\Phi c_t,\, \phi\Big) + \Big(D(\mathbf{u})\nabla c,\, \nabla\phi\Big) + \Big(\mathbf{u}\cdot\nabla c,\, \phi\Big) = \Big(\hat{c}q^I - cq^P,\, \phi\Big), \tag{11}$$

$$\Big(\mu(c)\mathbf{K}^{-1}\mathbf{u},\, \mathbf{v}\Big) = \Big(p,\, \nabla\cdot\mathbf{v}\Big), \tag{12}$$

$$\Big(\nabla\cdot\mathbf{u},\, \varphi\Big) = \Big(q^I - q^P,\, \varphi\Big), \tag{13}$$

for $(\phi,\varphi,\mathbf{v}) \in (H^1, H^1, \mathbf{H}_0^1(\mathrm{d}iv))$.

We define below the finite element spaces used in Galerkin-mixed methods. For a given partition $\mathcal{T}_h$, we denote the classical Lagrange finite element spaces by

$$V_h^r = \{v_h \in C^0(\Omega) : v_h|_K \in P_r(K), \quad \forall K \in \mathcal{T}_h\},$$

where P_r is the space of polynomials of degree $r \geq 1$. Here we focus our attention on the Raviart-Thomas mixed FEMs. Some other types of mixed FEMs can be found in literature [5, 33] and the extension of the current schemes to those mixed methods is straightforward. We define the Raviart-Thomas finite element spaces [5, 33] by

$$\begin{aligned}
&\mathbf{H}_h^k := \{\mathbf{v}_h \in \mathbf{H}(\mathrm{d}iv) : \mathbf{v}_h|_K \in [P_k(K)]^d + \mathbf{x}P_k(K), \quad \forall K \in \mathcal{T}_h\} \\
&S_h^k := \{v_h \in L^2 : v_h|_K \in P_k(K), \quad \forall K \in \mathcal{T}_h\}, \quad \widehat{S}_h^k := S_h^k/\{constants\}.
\end{aligned}$$

We denote by I_h the Lagrange nodal interpolation operator on these finite element spaces.

Euler-$GM(r,k)$ algorithm. A fully discrete linearized Euler Galerkin-mixed FEM (denoted by $GM(r,k)$) for $r \geq 1$ and $k \geq 0$ is to find $(c_h^n, p_h^n, \mathbf{u}_h^n) \in (V_h^r, \widehat{S}_h^k, \mathbf{H}_h^k)$, $n = 0, 1, \cdots, N$, such that for all $(\phi_h, \varphi_h, \mathbf{v}_h) \in (V_h^r, S_h^k, \mathbf{H}_h^k)$,

$$\begin{aligned} &\Big(\Phi D_t c_h^{n+1},\, \phi_h\Big) + \Big(D(\mathbf{u}_h^n)\nabla c_h^{n+1},\, \nabla\phi_h\Big) \\ &+ \Big(\mathbf{u}_h^n \cdot \nabla c_h^n,\, \phi_h\Big) = \Big(\hat{c}q^I - c_h^{n+1}q^P,\, \phi_h\Big), \end{aligned} \tag{14}$$

$$\Big(\mu(c_h^n)\mathbf{K}^{-1}\mathbf{u}_h^{n+1},\, \mathbf{v}_h\Big) = -\Big(p_h^{n+1},\, \nabla\cdot\mathbf{v}_h\Big), \tag{15}$$

$$\Big(\nabla\cdot\mathbf{u}_h^{n+1},\, \varphi_h\Big) = \Big(q^I - q^P,\, \varphi_h\Big), \tag{16}$$

where the initial data $c_h^0 = I_h c_0$. At each time step of the above algorithm, one only needs to solve the linear parabolic finite element system (14) for the concentration and the linear mixed system (15)-(16) for the velocity and pressure. These two systems are decoupled and the computation can be performed in parallel. Since the coefficient matrix of the system (14) is symmetric positive definite and the mixed system (15)-(16) defines a standard saddle point problem, the existence and uniqueness of the numerical solution follow immediately. Some slightly different schemes were investigated by several authors, *e.g.*, see [7, 13, 27]. Among these Galerkin-mixed methods, $GM(1,0)$ is most popular in applications, in which a linear approximation is used for the concentration and lowest-order (0-order) Raviart-Thomas element is used for the velocity and pressure.

The error analysis of the Galerkin-mixed methods was first studied in [12], in which the L^2-norm error estimate (5) was presented under certain time-step restriction and the mesh condition. In our recent work [37], theoretical analysis of the Galerkin-mixed method $GM(r, r-1)$ was investigated. In terms of an elliptic quasi-projection, the optimal error estimate of Euler-$GM(1,0)$ was established. It is not difficult to extend the analysis to the general case $r \geq 0$ to obtain the optimal L^2-norm error estimate

$$\|c^n - c_h^n\|_{L^2} \leq C(\tau + h^2) \tag{17}$$

$$\|\mathbf{u}^n - \mathbf{u}_h^n\|_{L^2} + \|p^n - p_h^n\|_{L^2} \leq C(\tau + h^{r+1}) \tag{18}$$

for Euler-$GM(r, r-1)$ method. One can see from the above estimates that the Galerkin-mixed method $GM(1,0)$ provides the second-order accuracy for the numerical concentration in the spatial direction, instead of $O(h)$ as presented in previous work [12, 13]. Moreover, the accuracy of numerical velocity/pressure by the $GM(r, r-1)$ method is one-order lower than that of numerical concentration. To obtain the numerical pressure and velocity with the same order accuracy at certain time level, we propose a $GM^+(r, r-1)$ algorithm below.

Euler-$GM^+(r, r-1)$ algorithm. We first solve the system (14)-(16) by the Galerkin-mixed method $GM(r, r-1)$ for $n = 1, 2, ..., N$. Then, with the obtained c_h^m, we resolve the velocity/pressure system (15)-(16) at $t = t_m$ by the Galerkin-mixed method $GM(r, r)$, *i.e.*, finding $(\widetilde{p}_h^m, \widetilde{\mathbf{u}}_h^m) \in (\widehat{S}_h^r, \mathbf{H}_h^r)$ such that

$$\Big(\mu(c_h^m)\mathbf{K}^{-1}\widetilde{\mathbf{u}}_h^m,\, \mathbf{v}_h\Big) = -\Big(\widetilde{p}_h^m,\, \nabla\cdot\mathbf{v}_h\Big), \tag{19}$$

$$\Big(\nabla\cdot\widetilde{\mathbf{u}}_h^m,\, \varphi_h\Big) = \Big(q^I - q^P,\, \varphi_h\Big). \tag{20}$$

Based on the estimate (18), we have the following error estimate for the Euler-$GM^+(r, r-1)$ algorithm.

Proposition 2.1. Let $(c_h^n, \widetilde{p}_h^m, \widetilde{\mathbf{u}}_h^m)$ be the solution of $GM^+(r, r-1)$ algorithm. Then

$$\max_n \|c_h^n - c^n\|_{L^2} + \|\widetilde{p}_h^m - p^m\|_{L^2} + \|\widetilde{\mathbf{u}}_h^m - \mathbf{u}^m\|_{L^2} \le C(\tau + h^{r+1}) \,. \tag{21}$$

As (19)-(20) defines a discrete elliptic system, they can be solved in parallel if numerical velocity/pressure at several time levels are required.

Crank-Nicolson-$GM(r, k)$ algorithm. To obtain a second-order accuracy in the time direction, we present a fully discrete linearized Crank-Nicolson $GM(r, k)$ methods, which is to find $(c_h^n, p_h^n, \mathbf{u}_h^n) \in (V_h^r, \widehat{S}_h^k, \mathbf{H}_h^k)$, $n = 2, 3, \cdots, N$, such that for all $(\phi_h, \varphi_h, \mathbf{v}_h) \in (V_h^r, S_h^k, \mathbf{H}_h^k)$,

$$\begin{aligned} &\Big(\Phi D_t c_h^n,\, \phi_h\Big) + \Big(D(\widehat{\mathbf{u}}_h^{n-1/2})\nabla c_h^{n-1/2},\, \nabla\phi_h\Big) \\ &+ \Big(\widehat{\mathbf{u}}_h^{n-1/2} \cdot \nabla c_h^{n-1/2},\, \phi_h\Big) = \Big(\hat{c} q^I - c_h^{n-1/2} q^P,\, \phi_h\Big), \end{aligned} \tag{22}$$

$$\Big(\mu(\widehat{c}_h^n)\mathbf{K}^{-1}\mathbf{u}_h^n,\, \mathbf{v}_h\Big) = -\Big(p_h^n,\, \nabla\cdot\mathbf{v}_h\Big), \tag{23}$$

$$\Big(\nabla\cdot\mathbf{u}_h^n,\, \varphi_h\Big) = \Big(q^I - q^P,\, \varphi_h\Big), \tag{24}$$

where

$$v^{n-1/2} = \frac{v^n + v^{n-1}}{2}$$

and $\widehat{\mathbf{u}}_h^{n-1/2}$ and $\widehat{c}_h^n$ denote the standard extrapolation by

$$\begin{aligned} \widehat{\mathbf{u}}^{n-1/2} &= \frac{1}{2}(3\mathbf{u}^{n-1} - \mathbf{u}^{n-2}) \\ \widehat{c}^n &= 2c^{n-1} - c^{n-2} \,. \end{aligned}$$

At the initial time step, we choose $\mathbf{u}_h^0 = I_h u_0$ and $(c_h^1, \mathbf{u}^1, p_h^1)$ can be calculated by the Euler-GM(r,k) algorithm.

The extension of the theoretical analysis given in [37] for the Euler-$GM(r, r-1)$ method to the Crank-Nicolson-$GM(r, r-1)$ method is straightforward. To obtain a more accurate numerical velocity and pressure, we propose the Crank-Nicolson-$GM^+(r, r-1)$ algorithm below.

Crank-Nicolson $GM^+(r, r-1)$ algorithm. With the obtained c_h^m by Crank-Nicolson-$GM(r, r-1)$ algorithm, a new numerical velocity/pressure $(\widetilde{p}_h^m, \widetilde{\mathbf{u}}_h^m) \in \widehat{S}_h^r \times \mathbf{H}_h^r$ can be obtained by resolving the following mixed system by $GM(r, r)$ method

$$\Big(\mu(c_h^m)\mathbf{K}^{-1}\widetilde{\mathbf{u}}_h^m,\, \mathbf{v}_h\Big) = -\Big(\widetilde{p}_h^m,\, \nabla\cdot\mathbf{v}_h\Big), \tag{25}$$

$$\Big(\nabla\cdot\widetilde{\mathbf{u}}_h^m,\, \varphi_h\Big) = \Big(q^I - q^P,\, \varphi_h\Big). \tag{26}$$

The following optimal error estimate holds for the Crank-Nicolson-$GM^+(r, r-1)$ algorithm.

Proposition 2.2. Let $(c_h^n, \widetilde{p}_h^m, \widetilde{\mathbf{u}}_h^m)$ be the solution of Crank-Nicolson-$GM^+(r, r-1)$ algorithm. Then

(27)
$$\max_n \|c_h^n - c^n\|_{L^2} + \|\widetilde{p}_h^m - p^m\|_{L^2} + \|\widetilde{\mathbf{u}}_h^m - \mathbf{u}^m\|_{L^2} \le C(\tau^2 + h^{r+1}), \quad \text{for } r \ge 1\,.$$

Remarks. The lowest-order Galerkin-mixed method $GM(1,0)$ is most popular in reservoir simulations and exploration of underground water and oil, while the previous analysis only showed the first-order convergence rate under certain conditions on time step and spatial mesh size. To get a high-order accuracy, one often use the Galerkin-mixed method $GM(r,r)$ $(r \ge 1)$ in some applications based on previous error estimate (5). From the new error analysis (10), the Galerkin-mixed method $GM(r, r-1)$ produces the same order convergence rate $O(h^{r+1})$ for the concentration as $GM(r,r)$ and one-order lower rate for the velocity/pressure. The method requires less computational cost since a lower-order mixed approximation is used for the pressure equation. The proposed $GM^+(r, r-1)$ algorithm shows the optimal convergence rate $O(h^{r+1})$ for all three components. Indeed, the proposed $GM^+(1,0)$ algorithm is more competitive both in efficiency and accuracy. In the following two sections, we shall present a systematic numerical simulation to further confirm the theoretical analysis in [37] in a more general case and show the accuracy and efficiency for the proposed $GM^+(r, r-1)$ algorithm in comparison with the classical $GM(r,r)$ method.

3. Numerical simulations for smooth solutions

In this section, we present numerical results for incompressible miscible flows in both two- and three-dimensional porous media to confirm theoretical analysis given in Propositions 1-2 and [37] and show the accuracy and efficiency of our algorithms. All computations in the following two sections are performed by using the software FEniCS [31].

Example 3.1. We rewrite the system (1)-(2) by

$$\frac{\partial c}{\partial t} - \nabla \cdot (D(\mathbf{u})\nabla c) + \mathbf{u} \cdot \nabla c = g, \tag{28}$$

$$\nabla \cdot \mathbf{u} = f, \tag{29}$$

$$\mathbf{u} = -\frac{\mathbf{K}}{\mu(c)}\nabla p \tag{30}$$

with the boundary/initial conditions defined in (3), where $D(\mathbf{u}) = I + |\mathbf{u}|^2/(1 + |\mathbf{u}|^2) + \mathbf{u} \otimes \mathbf{u}$ and $\mu(c) = 1 + c^2$.

First, we consider the two-dimensional model in $\Omega = [0,1] \times [0,1]$ with $\mathbf{K}$ being the identity matrix. We set the terminal time $T = 1.0$. The functions f, g and c_0 are chosen correspondingly to the exact solution

$$p = e^{-t}\cos(2\pi x)\cos(2\pi y), \tag{31}$$

$$c = \cos(\frac{\pi t}{3})(1 + \cos(2\pi x)\cos(2\pi y)), \tag{32}$$

which satisfies the boundary condition (3).

A uniform triangular mesh with M+1 vertices in each direction is used in this example, where $h = \frac{\sqrt{2}}{M}$ (see Figure 1 for the illustration with $M = 8$). We solve

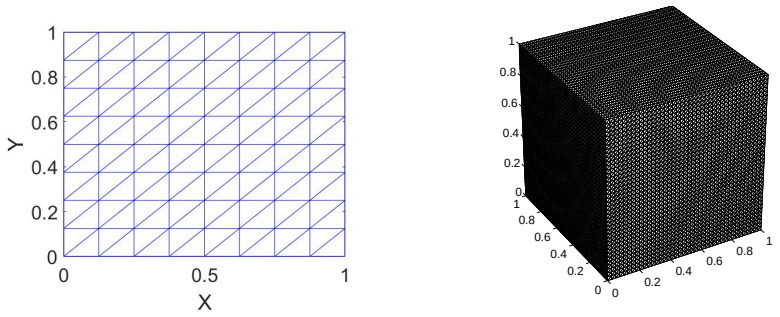

FIGURE 1. A uniform triangular/tetrahedron mesh on the unit square/cube.

the Euler discrete system (14)-(16) and the Crank-Nicolson discrete system (22)-(24) by $GM(r, r-1)$ and $GM(r, r)$ for $r = 1, 2$, respectively. With the obtained numerical concentration c_h^N from $GM(r, r-1)$ method, following the $GM^+(r, r-1)$ algorithm we resolve the system (19)-(20) and the system (25)-(26), respectively, to get a new numerical pressure and velocity $(\widetilde{p}_h^N, \widetilde{\mathbf{u}}_h^N)$. A general L^2-norm error is defined by

$$E_w = \max_{0\le n\le N} \|w(t_n, x) - w_h^n(x)\|_{L^2(\Omega)}, \quad E_{\widetilde{w}} = \|w(t_N, x) - \widetilde{w}_h^N\|_{L^2} \tag{33}$$

with $w = c, \mathbf{u}, p$.

TABLE 1. L^2-norm errors of Euler Galerkin-mixed FEMs (GM and GM^+) in 2D (Example 3.1).

	E_c	E_p	$E_{\mathbf{u}}$	E_c	E_p	$E_{\mathbf{u}}$	$E_{\widetilde{p}}$	$E_{\widetilde{\mathbf{u}}}$
$\tau = 16h^2$	$GM(1,0)$			$GM(1,1)$			$GM^+(1,0)$	
M=16	1.91e-01	3.67e-02	5.68e-01	2.27e-01	5.01e-02	6.52e-02	3.16e-02	3.86e-02
M=32	4.52e-02	8.97e-03	2.97e-01	5.55e-02	1.20e-02	1.84e-02	6.28e-03	1.02e-02
M=64	1.11e-02	2.23e-03	1.50e-01	1.37e-02	2.94e-03	4.72e-03	1.47e-03	2.73e-03
M=128	3.22e-03	8.19e-03	5.42e-02	3.42e-03	7.33e-04	1.19e-03	3.62e-04	6.87e-04
rate	2.03	1.04	0.98	2.02	2.03	1.93	2.14	1.94
$\tau = 64h^3$	$GM(2,1)$			$GM(2,2)$			$GM^+(2,1)$	
M=8	4.64e-02	5.75e-02	1.61e-01	5.45e-02	5.32e-02	7.78e-02	5.51e-03	1.09e-02
M=16	5.42e-03	8.83e-03	4.43e-02	6.30e-03	7.22e-03	1.15e-02	6.12e-04	1.36e-03
M=32	6.49e-04	1.54e-03	1.12e-02	7.19e-04	9.11e-04	1.47e-03	7.29e-05	1.66e-04
M=64	8.04e-05	3.31e-04	2.82e-03	8.50e-05	1.14e-04	1.85e-04	9.02e-06	2.08e-05
rate	3.06	2.08	1.95	3.11	2.96	2.91	3.08	3.01

TABLE 2. L^2-norm errors of Crank-Nicolson Galerkin-mixed FEMs (GM and GM^+) in 2D (Example 3.1).

	E_c	E_p	$E_{\mathbf{u}}$	E_c	E_p	$E_{\mathbf{u}}$	$E_{\widetilde{p}}$	$E_{\widetilde{\mathbf{u}}}$
$\tau = h/16$	$GM(1,0)$			$GM(1,1)$			$GM^+(1,0)$	
M=16	1.10e-01	6.52e-02	3.42e-01	1.58e-01	2.97e-02	2.82e-02	1.70e-02	9.78e-03
M=32	2.69e-02	3.27e-02	1.72e-01	3.90e-02	6.86e-03	7.07e-03	3.84e-03	2.43e-03
M=64	6.66e-03	1.63e-02	8.59e-02	9.68e-03	1.67e-03	1.77e-03	9.32e-04	6.07e-04
M=128	1.66e-03	8.18e-03	4.30e-02	2.42e-03	4.18e-04	4.43e-04	2.31e-04	1.52e-04
rate	2.03	1.00	1.00	2.01	2.16	1.98	2.15	2.01
$\tau = (\frac{h}{16})^{1.5}$	$GM(2,1)$			$GM(2,2)$			$GM^+(2,1)$	
M=16	7.68e-04	4.96e-03	4.43e-02	5.92e-04	2.76e-04	1.89e-03	1.41e-04	5.12e-04
M=32	6.97e-05	1.24e-03	1.12e-02	7.02e-05	3.45e-05	2.38e-04	1.41e-05	6.41e-05
M=64	1.10e-05	3.11e-04	2.82e-03	8.59e-05	4.32e-06	2.98e-05	1.61e-06	7.61e-06
rate	3.06	2.00	1.95	3.04	3.00	2.97	3.23	3.04

For comparison, we take the time-step $\tau = Ch^{r+1}$ for Euler-$GM(r, r-1)$ and Euler-$GM(r, r)$ and $\tau = Ch^{(r+1)/2}$ for the corresponding Crank-Nicolson schemes with $r = 1, 2$ in our computation. We present in Table 1 the L^2-norm errors of numerical concentration, pressure and velocity obtained by these six Euler-type methods. The corresponding numerical results by Crank-Nicolson scheme are presented in Table 2. Several observations are as follows.

• Numerical results in Table 1 show clearly that all these six methods provide optimal accuracy for each of three components, concentration, pressure and velocity with the convergence rate

$$\|c^n - c_h^n\|_{L^2} + \|p^n - p_h^n\|_{L^2} + \|\mathbf{u}^n - \mathbf{u}_h^n\|_{L^2} \le C(\tau + h^{r+1}) \tag{34}$$

for $GM(r, r)$ and

$$\|c^n - c_h^n\|_{L^2} + h(\|p^n - p_h^n\|_{L^2} + \|\mathbf{u}^n - \mathbf{u}_h^n\|_{L^2}) \le C(\tau + h^{r+1}) \tag{35}$$

for $GM(r, r-1)$. The former was proved theoretically in [12, 13] under the time step condition $\tau = o(h)$ and the spatial mesh condition (6) and in [27] for $r > 0$ unconditionally. The latter was shown in [37] unconditionally. On the other hand, the mesh-size restriction in (8) seems not necessary. From Table 2, the corresponding Crank-Nicolson Galerkin-mixed methods provide the same accuracy in the spatial direction.

• Numerical pressure and velocity given by $GM(r, r)$ are more accurate than by $GM(r, r-1)$ since a higher-order mixed approximation has been used for the pressure/velocity. However, there is no much difference between numerical concentrations obtained by these two methods and both are in the order of $O(h^{r+1})$. Clearly the concentration is a more important component in applications. The $GM(r, r)$ method requires a higher computational cost at each time step. Moreover, our results also show that for the Euler-$GM(r, r-1)$ method, the one-order lower approximation to $(p, \mathbf{u})$ does not pollute the numerical concentration, although the system is nonlinear and strongly coupled.

• The proposed $GM^+(r, r-1)$ algorithm is based on the $GM(r, r-1)$ algorithm and a refined solution of the pressure equation by a high-order mixed method at the time level $t = t_N$. The algorithm produces the optimal convergence rate as given in (21) for all three components. After resolving the pressure equation, the accuracy of numerical pressure and velocity gets much improved, even better than results from $GM(r, r)$, while in the latter, a higher-order mixed approximation is used for the pressure equation at all time levels and more computational cost is required. Therefore, the proposed algorithm shows better performance in both accuracy and efficiency.

• Due to the nature of the discontinuity of media in applications, the $GM(1, 0)$ method is most popular. The previous analysis given in [12, 13] only showed the first-order accuracy for all three components in L^2-norm. The second-order accuracy of the numerical concentration was established in [37], which is confirmed by our numerical results. Moreover, the proposed $GM^+(1, 0)$ algorithm shows the second-order accuracy for all three components.

Example 3.2. Secondly we consider the incompressible miscible flow in a three-dimensional porous medium, described by the system (31)-(32) in the unit cube $\Omega = [0, 1]^3$. Similarly we set the terminal time $T = 1.0$ and the functions f, g and

c_0 are chosen correspondingly to the exact solution

$$p = e^{-t}\cos(2\pi x)\cos(2\pi y)\cos(2\pi z), \tag{36}$$

$$c = \cos(\frac{\pi t}{3})(1+\cos(2\pi x)\cos(2\pi y)\cos(2\pi z)), \tag{37}$$

which satisfies the boundary condition (3).

We use a uniform partition with M+1 vertices in each direction, where $h = \frac{\sqrt{3}}{M}$ (see Figure 1 for the illustration). We solve the Euler system (14)-(16) and the Crank-Nicolson system (22)-(24) by $GM(1,0)$ and $GM(1,1)$, respectively. With the obtained numerical concentration c_h^N, we follow the $GM^+(1,0)$ algorithm and resolve the system (19)-(20) to get a new numerical pressure $\widetilde{p}_h^N$ and velocity $\widetilde{\mathbf{u}}_h^N$. For comparison, we present in Table 3 numerical errors of Euler-$GM(1,0)$, Euler-$GM^+(1,0)$, Crank-Nicolson-$GM(1,0)$ and Crank-Nicolson-$GM^+(1,0)$ algorithms. Again, we can see from Table 3 that the $GM(1,0)$ algorithm provides the second-order accuracy in the spatial direction for the concentration and the $GM^+(1,0)$ algorithm shows the second-order accuracy for all three components.

TABLE 3. L^2-norm errors of Euler/Crank-Nicolson Galerkin-mixed FEMs (GM and GM^+) in 3D (Example 3.2).

Euler	$GM(1,0)$			$GM^+(1,0)$	
$\tau = 16h^2$	E_c	E_p	$E_{\mathbf{u}}$	$E_{\widetilde{p}}$	$E_{\widetilde{\mathbf{u}}}$
M=8	4.37e-02	4.60e-02	2.22e-01	2.07e-03	7.08e-03
M=16	1.17e-02	2.41e-02	1.16e-01	5.09e-04	1.78e-03
M=32	2.99e-03	1.22e-02	5.88e-02	1.27e-04	4.46e-04
rate	1.94	0.96	0.96	2.01	1.99
Crank-Nicolson	$GM(1,0)$			$GM^+(1,0)$	
$\tau = h/16$	E_c	E_p	$E_{\mathbf{u}}$	$E_{\widetilde{p}}$	$E_{\widetilde{\mathbf{u}}}$
M=8	4.24e-02	4.73e-02	2.29e-01	2.04e-03	7.07e-03
M=16	1.10e-02	2.41e-02	1.16e-01	4.96e-04	1.78e-03
M=32	2.76e-03	1.22e-02	5.86e-02	1.23e-04	4.45e-04
rate	1.97	0.98	0.98	2.03	2.00

4. Numerical simulations for non-smooth solutions

In this section, we study two examples with non-smooth solutions.

Example 4.1. We consider the system (28)-(30) in a two-dimensional L-shaped domain. The solution around the reentrant corner is not smooth. Here the functions f, g and c_0 are chosen correspondingly to the exact solution

$$c = \left[1 + (1+x^2)(1-x^2)^2(1+y^2)(1-y^2)^2 r^{2/3}\cos\frac{2\theta}{3}\right](2-t^2) \tag{38}$$

$$p = (1+x^2)(1-x^2)^2(1+y^2)(1-y^2)^2 r^{2/3}\cos\frac{2\theta}{3}\cos\frac{\pi t}{3}\,. \tag{39}$$

We see that

$$c \in H^{1+s}, \quad p \in H^{1+s}, \quad \mathbf{u} \in \mathbf{H}^s, \qquad \text{for } s < 2/3\,. \tag{40}$$

Theoretical analysis for the problem in a non-convex domain was not done, although the optimal error estimate under the assumption of the solution being smooth was presented in [37]. Based on the regularity of the solution and classical interpolation error estimates, the expected optimal error estimate in the spatial

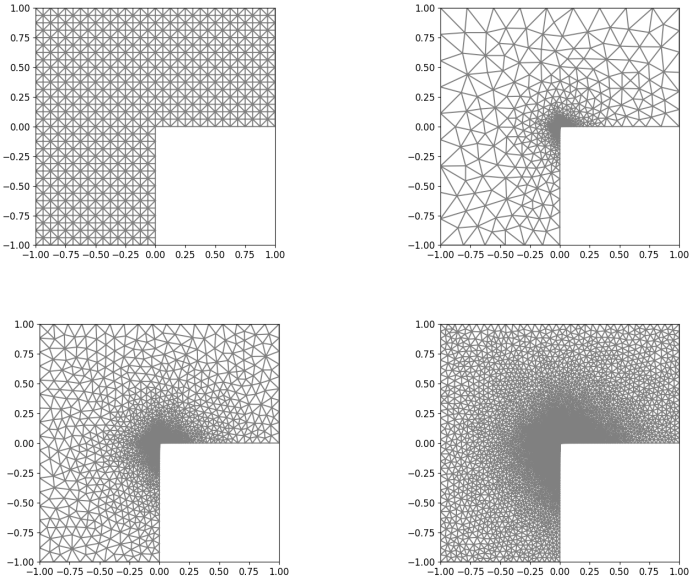

FIGURE 2. Top Left: the uniform mesh with $M = 16$. Top Right: the first mesh with 1010 nodes and 2024 elements. Bottom Left: the second mesh with 4020 nodes and 8044 elements. Bottom Right: the third mesh with 16138 nodes and 32280 elements.

direction is

$$\|c - c_h\|_{L^2} = O(h^{2s})$$
$$\|p - p_h\|_{L^2} = O(h)$$
$$\|\mathbf{u} - \mathbf{u}_h\|_{L^2} = O(h^s)$$

for Euler-$GM(1,0)$ algorithm and

$$\|p - \widetilde{p}_h\|_{L^2} = O(h^{2s})$$
$$\|\mathbf{u} - \widetilde{\mathbf{u}}_h\|_{L^2} = O(h^s)$$

for Euler-$GM^+(1,0)$ algorithm. We present in Table 4 the L^2-norm error of Euler-$GM(1,0)$ and Euler-$GM^+(1,0)$ algorithms on a uniform mesh. We observe from Table 4 that numerical results are in good agreement with the prediction above. Numerical results are improved in all cases by using Euler-$GM^+(1,0)$ algorithm. The convergence rate for the pressure increases from $O(h)$ to $O(h^{2s})$, while the convergence rate for the velocity is unchanged due to its weak regularity. The convergence rate of the numerical concentration for both algorithms is in the order $2s$ which is even better than the rate shown in previous analysis [12, 13] under a smooth setting.

Clearly the regularity of the exact solution near the reentrant corner of the L-shape is not enough to get a second order convergence for the linear FEM on a uniform mesh. It has been noted that a local refinement may improve the convergence rate further. Here we test our algorithms with locally refined meshes. We present three non-uniform meshes in Figure 2 with a finer mesh distribution

around the reentrant corner. These three meshes are generated by the software Gmsh [24] with six specified element-size parameters at each corner of the polygon. In order to test the convergence rate in the spatial direction, we set $\tau = 16/N_t$ and we present the L^2-norm errors of both Euler-$GM(1,0)$ and Euler-$GM^+(1,0)$ algorithms in Table 4, where N_t denotes the number of total unknowns. One can observe that the optimal rates in L^2-norm for all three components are achieved, *i.e.*, the second order (proportional to N_t) for c_h, $\widetilde{p}_h$ and $\widetilde{\mathbf{u}}_h$ and the first order for p_h and $\mathbf{u}_h$.

TABLE 4. L^2-norm errors of Euler Galerkin-mixed FEMs (GM and GM^+) in 2D L-shape (Example 4.1).

$\tau = 1/M^2$	No.of unknowns	$GM(1,0)$			$GM^+(1,0)$	
Uniform mesh	N_t	E_c	E_p	$E_{\mathbf{u}}$	$E_{\widetilde{p}}$	$E_{\widetilde{\mathbf{u}}}$
M=16	833	9.98e-03	1.80e-02	3.26e-02	8.60e-04	7.80e-03
M=32	3201	3.55e-03	8.78e-03	1.79e-02	3.22e-04	4.84e-03
M=64	12545	1.29e-03	4.32e-03	1.01e-02	1.24e-04	3.04e-03
rate		1.48	1.03	0.83	1.39	0.68
expected rate		1.33	1.0	0.67	1.33	0.67
$\tau = 64/N_t$	No.of unknowns	$GM(1,0)$			$GM^+(1,0)$	
Refined mesh	N_t	E_c	E_p	$E_{\mathbf{u}}$	$E_{\widetilde{p}}$	$E_{\widetilde{\mathbf{u}}}$
mesh 1	1010	1.02e-01	3.16e-02	5.51e-02	1.03e-02	7.02e-03
mesh 2	4020	2.43e-02	1.70e-02	2.95e-02	2.53e-03	2.15e-03
mesh 3	16138	5.99e-03	8.63e-03	1.51e-02	6.30e-04	5.66e-04
rate		2.05	0.98	0.97	2.02	1.93
expected rate		2.0	1.0	1.0	2.0	2.0

Example 4.2. Finally, we study a physical problem described by the system (1)-(3) with several different settings, including large mobility ratios, anisotropic dispersion, discontinuous permeability and porosity and point sources and sinks. Numerical experiments simulate miscible displacement within a horizontal reservoir of a thickness of one unit and a spatial domain $\Omega = (0, 1000) \times (0, 1000) ft^2$ over a period of 10 years. An injection well is located at the upper-right corner $(1000, 1000)$ with the injection rate $q^I = 30 ft^2/day$ and the injection concentration $\hat{c} = 1.0$. A production well is put at the lower-left corner $(0, 0)$ with the production rate $q^P = 30 ft^2/day$. The initial concentration $c_0(x, y) = 0$.

Here the viscosity is defined by

$$\mu(c) = \mu(0) \Big(1 + (M_r^{1/4} - 1)c\Big)^{-4}, \tag{41}$$

where M_r denotes the mobility ratio between the resident and injected fluids and $\mu(0)$ denotes the viscosity of resident fluid. The diffusion-dispersion tensor is defined by

$$\mathbf{D}(\mathbf{u}) = \Psi\Big(d_m \mathbf{I} + |\mathbf{u}|(d_l \mathbf{E}(\mathbf{u}) + d_t(\mathbf{I} - \mathbf{E}(\mathbf{u})))\Big), \tag{42}$$

where d_m denotes the molecular diffusion coefficient, d_l and d_t denotes the constant longitudinal and transversal dispersivities of the isotropic porous medium, respectively, $\mathbf{E}(\mathbf{u}) = \left(\frac{u_i u_j}{|\mathbf{u}|^2}\right)_{1 \le i,j \le 2}$ and $\mathbf{I}$ is the 2×2 identity matrix.

The problem was studied in [39] using the ELLAM-MFEM and later, by many authors, such as see [3, 8], using different methods. Here we consider the following

two different tests with the same parameters as given in [3, 39],

$$\text{Test I} \quad \begin{cases} \mathbf{K} = 80\mathbf{I},\ \Psi = 0.1,\ M_r = 41,\ \mu(0) = 1cp, \\ d_m = 0ft^2/day,\ d_l = 50ft,\ d_t = 5ft, \end{cases}$$

$$\text{Test II} \quad \begin{cases} \mathbf{K} = 80\mathbf{I} \text{ on } (0,1000) \times (0,500), \\ \mathbf{K} = 20\mathbf{I} \text{ on } (0,1000) \times (500,1000),\ \Psi = 0.1,\ M_r = 41,\ \mu(0) = 1cp, \\ d_m = 0ft^2/day,\ d_l = 50ft,\ d_t = 5ft, \end{cases}$$

In our numerical simulations, we use a standard uniform partition as shown in Figure 1 with $h = 10ft$ and a uniform time step $\tau = 120days$ (4 months). Numerical results reported here are based on the proposed Galerkin-mixed algorithm $GM^+(1,0)$. Numerical simulations with finer spatial meshes and smaller time steps were made to further verify our numerical results. We present in Figure 3 the surface and contour plots of the concentration for Test I at $t = 1, 3, 5, 7, 10$ years. Due to the nature of the physical model, the fluid flow moves mainly along the diagonal direction from the injection well to the production well. Because of the effect of the no-flow boundary condition and the production well, one can observe a clear interface and a channel of a fixed angle to the production well, which leads to a large variation of the concentration around the production well and therefore, a large variation of the viscosity $\mu(c)$ across the interface. Since the molecular diffusion coefficient $d_m = 0$ in this test, the problem is degenerate and the magnitude of the velocity is greater along the diagonal direction between the injection and production wells. From a qualitative point of view, the patterns shown in the Figure 3 are similar to those presented in [39]. We refer readers to [17, 39] for detailed physical description on these aspects.

The results for the Test II are presented in Figure 4 for $t = 1, 3, 5, 7, 10$ years. In this case, the permeability is discontinuous and the permeability in the lower half domain is greater than that in the upper half domain. Thus in the first year, the contour and surface plots are similar to those in Test I since the fluid is still in the half domain. However, when the fluid reaches the higher permeability domain, that is, the lower half domain, it moves faster in the horizontal direction compared with the fluid in the upper half domain. These effects are illustrated by the contour and surface plots in Figure 4.

5. Conclusions

We have proposed a Galerkin-mixed algorithm for a nonlinear and strongly coupled parabolic system from incompressible miscible flow in porous media, which is based on classical Galerkin-mixed methods with certain combination of finite element spaces. The algorithm is more efficient due to the use of a lower-order mixed approximation for the time-dependent concentration equations and a post-processing technique for the elliptic pressure equation. Our numerical experiments have been presented for a more general case with both smooth and non-smooth solutions. Numerical results show that the algorithm provides optimal accuracy for all three physical components. In particular, based on the most commonly-used lowest-order Galerkin-mixed approximation, the algorithm provides the second order convergence rate $O(h^2)$ for the solution being smooth and the problem in a non-convex polygon with local refined meshes. Theoretical analysis of the second-order convergence rate for the concentration was presented in our recent [37] under the assumption of the solution being smooth. All other previous works only proved the first-order accuracy under certain time-step restriction and the mesh-size condition, excluding more practical case $h = h_p = h_c$. More important is that nonlinear

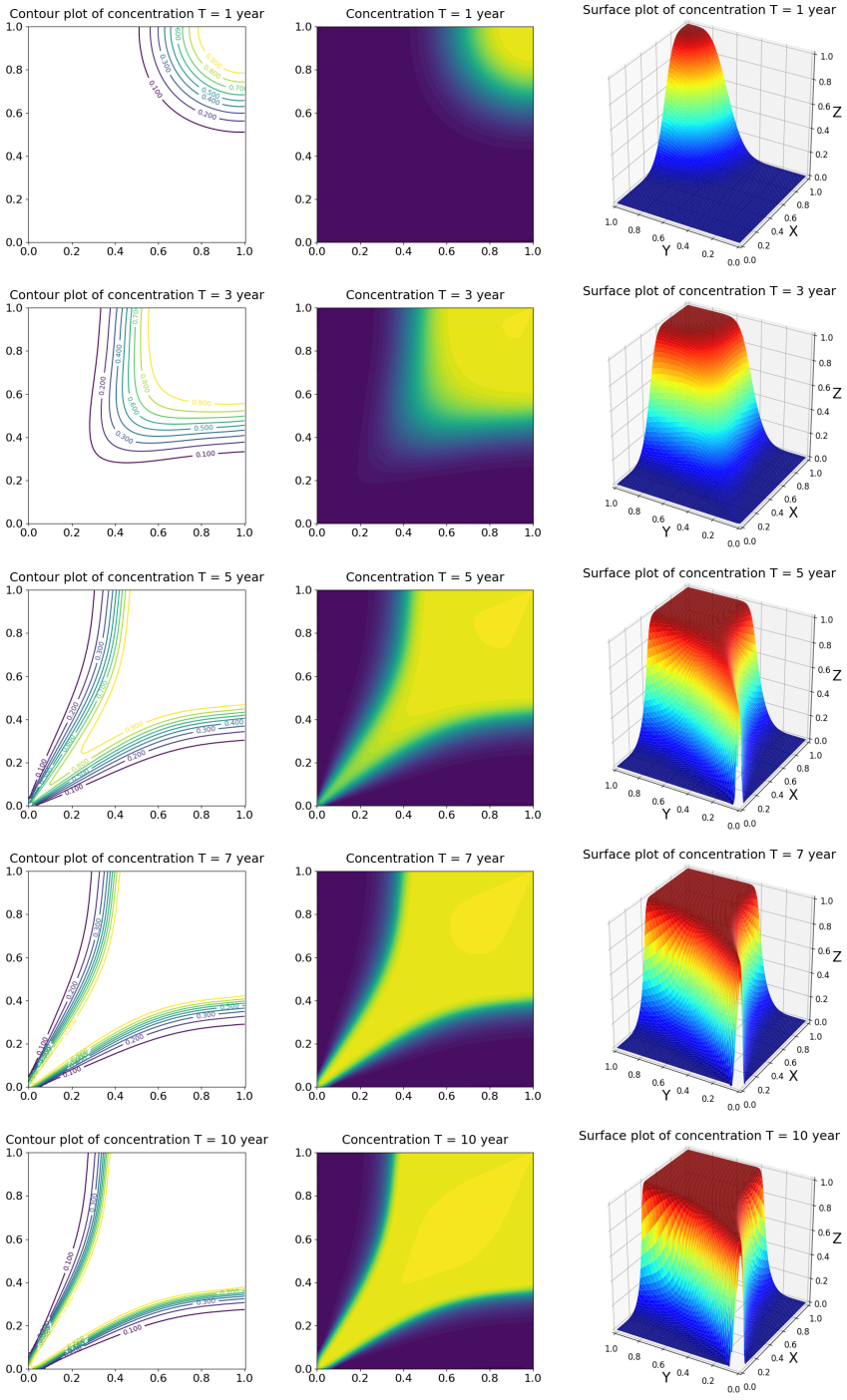

FIGURE 3. Continuous permeability (Test I, $T = 10$ year).

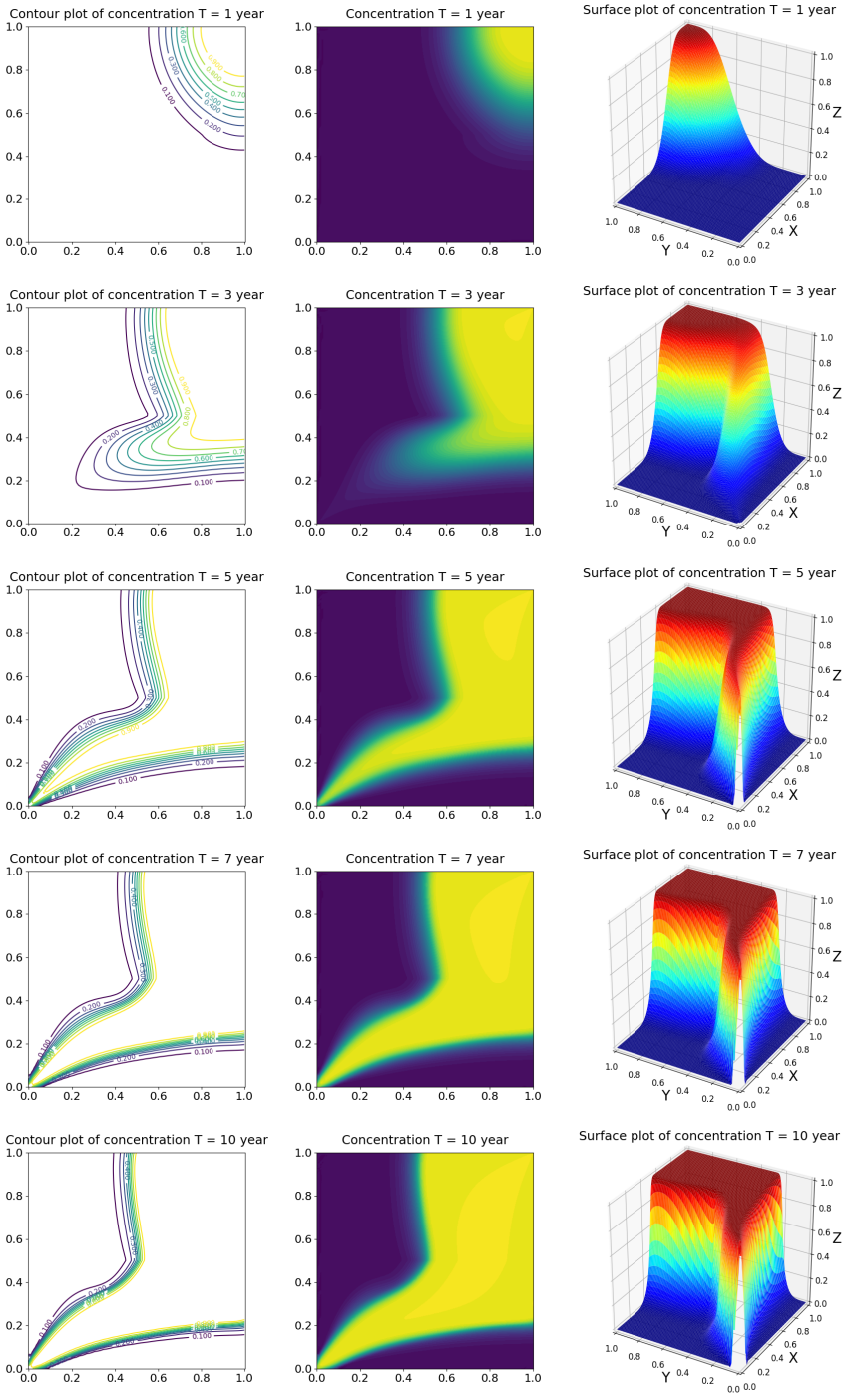

FIGURE 4. Discontinuous permeability (Test II, $T = 10$ year).

coupled parabolic systems can be found in many applications [2, 16, 29, 42, 44, 45], in which existing numerical methods often require a higher-order approximation to one component, It is possible to extend our algorithm to these models to obtain optimal error estimates for all components.

Acknowledgments

The work of the authors was supported in part by a grant from Beijing Normal University at Zhuhai and a grant from the Research Grants Council of the Hong Kong Special Administrative Region, China (Project No. CityU 11300517).

References

[1] B. Amaziane and M. El Ossmani, Convergence analysis of an approximation to miscible fluid flows in porous media by combining mixed finite element and finite volume methods, *Numer. Methods Partial Diff. Eq.*, 24 (2008), pp. 799–832.

[2] R. An and J. Su, Optimal error estimates of semi-implicit Galerkin method for time-dependent Nematic liquid crystal flows, *J. Scientific Computing*, 74(2018), pp. 979–1008.

[3] D. Anderson and J. Droniou, An arbitrary-order scheme on generic meshes for miscible displacements in porous media, *SIAM J. Sci. Comput.*, 40(2018), pp. B1020–B1054.

[4] J. Bear and Y. Bachmat, *Introduction to Modeling of Transport Phenomena in Porous Media*, Springer-Verlag, New York, 1990.

[5] S. Brenner and L. Scott, *The Mathematical Theory of Finite Element Methods*, Springer, New York, 2002.

[6] C. Chainais-Hillairet and J. Droniou, Convergence analysis of a mixed finite volume scheme for an elliptic-parabolic system modeling miscible fluid flows in porous media, *SIAM J. Numer. Anal.*, 45.5(2007), pp. 2228–2258.

[7] F. Chen, H. Chen and H. Wang, An optimal-order error estimate for a Galerkin-mixed finite-element time-stepping procedure for porous media flows, *Numer. Methods Partial Differ. Equations*, 28.2(2012), pp. 707–719.

[8] H.M. Cheng and J. Droniou, An HMM-ELLAM scheme on generic polygonal meshes for miscible incompressible flows in porous media, *J. Petrol. Sci. Eng.*, 172(2018), pp. 707–723.

[9] A. Cheng, K. Wang and H. Wang, Superconvergence for a time-discretization procedure for the mixed finite element approximation of miscible displacement in porous media, *Numer. Methods Partial Differ. Equations*, 28(2012), pp. 1382–1398.

[10] B.L. Darlow, R. Ewing, M.F. Wheeler, Mixed finite element method for miscible displacement problems in porous media, *SPE. J.*, 24(1984), pp. 391–398.

[11] C.N. Dawson, T.F. Russell and M.F. Wheeler, Some improved error estimates for the modified method of characteristics, *SIAM J. Numer. Anal.*, 26 (1989), pp. 1487-1512.

[12] J. Douglas, JR., R.E. Ewing and M.F. Wheeler, The approximation of the pressure by a mixed method in the simulation of miscible displacement, *RAIRO Analyse numérique*, 17(1983), pp. 17–33.

[13] J. Douglas, JR., R. Ewing and M.F. Wheeler, A time-discretization procedure for a mixed finite element approximation of miscible displacement in porous media, *RAIRO Anal. Numer.*, 17 (1983), pp. 249–265.

[14] J. Douglas, JR., F. Furtada, and F. Pereira, On the numerical simulation of waterflooding of heterogeneous petroleum reservoirs, *Comput. Geosciences*, 1(1997), pp. 155–190.

[15] R.G. Durán, On the approximation of miscible displacement in porous media by a method of characteristics combined with a mixed method, *SIAM J. Numer. Anal.*, 25 (1988), pp. 989–1001.

[16] V.J. Ervin, W.W. Miles, Approximation of time-dependent viscoelastic fluid flow: SUPG approximation, *SIAM J. Numer. Anal.*, 41(2003), pp. 457–486.

[17] R.E. Ewing, ed, *The mathematics of Reservoir Simulation*, Frontiers in Applied Mathematics, SIAM, Philadelphia, PA, 1983.

[18] R.E. Ewing and M.F. Wheeler, Galerkin methods for miscible displacement problems in porous media, *SIAM J. Numer. Anal.*, 17 (1980), pp. 351–365.

[19] R.E. Ewing, T.F. Russell and M.F. Wheeler, Simulation of miscible displacement using mixed methods and a modified method of characteristics, *SPE 12241*, 1983, pp. 71–81.

[20] R.E. Ewing, T.F. Russell and M.F. Wheeler, Convergence analysis of an approximation of miscible displacement in porous media by mixed finite elements and a modified method of characteristics, *Comput. Methods Appl. Mech. Engrg.*, 47 (1984), pp. 73–92.
[21] R. E. Ewing and H. Wang, A summary of numerical methods for time-dependent advection-dominated partial differential equations, *J. Comput. Appl. Math.*, 128 (2001), pp. 423–445.
[22] X. Feng, On existence and uniqueness results for a coupled system modeling miscible displacement in porous media, *J. Math. Anal. Appl.*, 194 (1995), pp. 883–910.
[23] X. Feng and M. Neilan, A modified characteristic finite element method for a fully nonlinear formulation of the semigeostrophic flow equations, *SIAM J. Numer. Anal.*, 47 (2009), pp. 2952–2981.
[24] C. Geuzaine and J.F. Remacle, Gmsh: a three-dimensional finite element mesh generator with built-in pre- and post-processing facilities, *Int. J. Numer. Mesh. Engng.*, 79(2009), pp. 1309–1331.
[25] B. Li, J. Wang and W. Sun, The stability and convergence of fully discrete Galerkin-Galerkin FEMs for porous medium flows, *Commun. Comput. Phys.*, 15(2014), pp. 1141–1158.
[26] B. Li and W. Sun, Error analysis of linearized semi-implicit Galerkin finite element methods for nonlinear parabolic equations, *Int. J. Numer. Anal. & Modeling*, 10 (2013), 622–633.
[27] B. Li and W. Sun, Unconditional convergence and optimal error estimates of a Galerkin-mixed FEM for incompressible miscible flow in porous media, *SIAM J. Numer. Anal.*, 51(2013), pp. 1959–1977.
[28] B. Li and W. Sun, Regularity of the diffusion-dispersion tensor and error analysis of FEMs for a porous media flow, *SIAM J. Numer. Anal.*, 53(2015), pp. 1418–1437.
[29] B. Li and W. Sun, *Maximal L^p error analysis of FEMs for nonlinear parabolic equations with nonsmooth coefficients,* Int. J. Numer. Anal. Modeling, 14 (2017), pp. 670–687.
[30] P. Lin and D. Yang, An iterative perturbation method for the pressure equation in the simulation of miscible displacement in porous media, *SIAM J. Sci. Comput.*, 19(1998), pp. 893–911.
[31] A. Logg, K. Mardal and G. Wells (Eds.), *Automated Solution of Differential Equations by the Finite Element Method*, Springer, Berlin, 2012.
[32] S.M.C. Malta, and A.F.D. Loula, Numerical analysis of finite element methods for miscible displacement in porous media, *Numer. Methods for Partial Differential Eq.*, 14 (1998), pp. 519–548.
[33] P.A. Raviart and J.M. Thomas, A mixed finite element method for 2nd order elliptic problems, *Mathematical Aspects of Finite Element Methods*, 606(1977), pp. 292–315.
[34] A.E. Scheidegger, *The physics of flow through porous media*, The MacMillan Company, New York, 1957.
[35] G. Scovazzi, M.F. Wheeler, A. Mikelić and S. Lee, Analytical and variational numerical methods for unstable miscible displacement flows in porous media, *J. Comput. Phys.*, 335(2017), pp. 444–496.
[36] S. Sun and M.F. Wheeler, Discontinuous Galerkin methods for coupled flow and reactive transport problems, *Applied Numer. Math.*, 52(2005), pp. 273–298.
[37] W. Sun and C. Wu, New analysis of Galerkin-mixed FEMs for for incompressible miscible flow in porous media, arXiv:2002.04820[math.NA].
[38] H. Wang, An optimal-order error estimate for a family of ELLAM-MFEM approximations to porous medium flow, *SIAM J. Numer. Anal.*, 46 (2008), pp. 2133–2152.
[39] H. Wang, D. Liang, R. E. Ewing, S. L. Lyons, and G. Qin, An approximation to miscible fluid flows in porous media with point sources and sinks by an Eulerian-Lagrangian localized adjoint method and mixed finite element methods, *SIAM J. Sci. Comput.*, 22 (2000), pp. 561–581.
[40] H. Wang, W. Zhao, M.S. Espedal and A.S. Telyakovskiy, A component-based Eulerian-Lagrangian formulation for multicomponent multiphase compositional flow and transport in porous media, *SIAM J. Sci. Comput.*, 35(2013), pp. B462–B486
[41] J. Wang, Z. Si and W. Sun, A new error analysis of characteristics-mixed FEMs for miscible displacement in porous media, *SIAM J. Numer. Anal.*, 52(2014), pp. 3300–3020.
[42] C. Wu and W. Sun, Analysis of Galerkin FEMs for a mixed formulation of Ginzburg-Landau equations under temporal gauge, *SIAM J. Numer. Anal.*, 56(2018), 1291–1312.
[43] C. Wu and W. Sun, New analysis of Galerkin FEMs for miscible displacement in porous media, *J. Sci. Computing*, 80(2019), 903–923.

[44] J. Yang, A posteriori error of a discontinuous Galerkin scheme for compressible miscible displacement problems with molecular diffusion and dispersion, *Int. J. Numer. Methods Fluids*, 65(2011), pp. 781–797.
[45] H. Zheng, J. Yu and L. Shan, Unconditional error estimates for time dependent viscoelastic fluid flow, *Appl. Numer. Math.*, 119(2017), pp. 1–17.

Advanced Institute of Natural Sciences, Beijing Normal University at Zhuhai, 519087, P.R. China and Division of Science and Technology, United International College, Zhuhai, P. R. China
E-mail: maweiw@uic.edu.hk

Department of Mathematics, City University of Hong Kong, Kowloon, Hong Kong, P.R. China
E-mail: chengda.wu@my.cityu.edu.hk